

Active electrocaloric demonstrator for direct comparison of PMN-PT bulk and multilayer samples

P. Blumenthal, C. Molin, S. Gebhardt & A. Raatz

To cite this article: P. Blumenthal, C. Molin, S. Gebhardt & A. Raatz (2016) Active electrocaloric demonstrator for direct comparison of PMN-PT bulk and multilayer samples, *Ferroelectrics*, 497:1, 1-8, DOI: [10.1080/00150193.2016.1160466](https://doi.org/10.1080/00150193.2016.1160466)

To link to this article: <http://dx.doi.org/10.1080/00150193.2016.1160466>



Published online: 05 May 2016.



Submit your article to this journal [↗](#)



Article views: 7



View related articles [↗](#)



View Crossmark data [↗](#)

Active electrocaloric demonstrator for direct comparison of PMN-PT bulk and multilayer samples

P. Blumenthal^a, C. Molin^b, S. Gebhardt^b, and A. Raatz^a

^aInstitute of Assembly Technology, Leibniz Universität Hannover, Garbsen, Germany; ^bFraunhofer Institute for Ceramic Technologies and Systems (IKTS), Dresden, Germany

ABSTRACT

One potential use of ferroelectrics is as active material in electrocaloric cooling systems. These systems promise a more energy efficient cooling process than vapor compression, thermoelectric or other current cooling systems. Currently different design types of electrocaloric cooling devices are in the focus of research. In this paper, we present an electrocaloric cooling device demonstrator working as “Active Electrocaloric Regenerator” (AER) and employing relaxor ferroelectric elements as active material. The device design is such that it allows the integration of different material systems and regenerator designs as well as a broad variation of operational parameters.

ARTICLE HISTORY

Received 28 June 2015
Accepted 12 November 2015

KEYWORDS

AER; electrocaloric; cooling device; PMN-PT; MLC

1. Introduction

The adiabatic temperature change of a dielectric material upon application or removal of an electrical field is called the electrocaloric effect (ECE). The existence of the ECE was theoretically explained already in 1878 [1], practically shown in Rochelle salt in 1930 [2] and experimentally determined for other materials from the 1950s. Unfortunately, the temperature changes observed in the assessed materials were limited to few Kelvin resulting in only little interest in the ECE. However, with the discovery of the giant electrocaloric effect in 2006 [3] (i.e. a temperature change of $\Delta T = 12$ K upon application of an electric field $\Delta E = 48$ kV/mm at 226 °C) potential for the use of the ECE in cooling applications (e.g. chip-cooling, battery-cooling) was identified and interest in this field rapidly increased.

To establish a cooling cycle and transport heat from a colder heat source to a hotter heat sink, basically four steps have to be periodically repeated: 1) Polarization of electrocaloric (EC) material, 2) Transfer of heat from EC material to heat sink, 3) Depolarization of EC material and 4) Transfer of heat from source to EC material. There are several different methods to realize this cooling cycle in practice. Two of these methods are currently very prominent: direct thermal contact in Solid-State Devices (SSD) (e.g. [4]) and fluidic heat transfer in Active Electrocaloric Regenerators (AER) (e.g. [5]). Especially challenging in Solid-State Devices is the efficient coupling and decoupling of EC elements to heat source/sink. Although there are different approaches to that challenge (e.g. using thermal switches

CONTACT P. Blumenthal  Blumenthal@match.uni-hannover.de

Color versions of one or more of the figures in the article can be found online at www.tandfonline.com/gfer.

© 2016 Taylor & Francis Group, LLC

[4] or actuated elements), no device demonstrator has been presented so far. However, SSD offer a large application potential (compact design, avoidance of additional thermal masses as fluids, prospectively high switching frequencies, quiet operation), making them one of the most regarded cooling device type. The prominence of the AER is due to the good thermal contact between heat transfer fluid and heat source, heat sink and EC elements as well as the internal regeneration, which facilitates an overall temperature gradient between heat source and sink that is larger than the inherent ECE of the active material. AER devices are the only device type which has been realized albeit only in a few prototypes [6, 7, 8]. There is still a lot of research demand ranging from regenerator design, materials and operational parameters to system evaluation.

The cooling device design presented in this paper is based on the AER. The detailed function principle, design and setup are explained in the subsequent section. On the one hand, the function principle is demonstrated in practice with this device. On the other hand, the particular setup allows a direct comparison of different active material systems, regenerator designs and operating parameters. Further, this device demonstrator is part of a larger investigation of the application of EC cooling systems for battery systems [9]. Therefore, components are designed for operation at around 40°C. For initial investigation, we employ lead magnesium niobate-lead titanate (PMN-PT), which is among the most promising material systems for EC cooling systems. Contrary to other applications of PMN-PT in EC cooling (e.g. [7]), we use multilayer structures instead of bulk samples. These multilayers promise two advantages. First, dielectric strength is expected to increase with reduction of layer thickness [10]. Second, the reduced operation voltage required to achieve the desired fields facilitates practical application. The setup and experimental validation of the designed AER device is demonstrated in the last section of the paper.

2. Cooling device design

The AER is the most widely known and regarded device type for EC cooling so far. It mainly consists of a fluidic bed with an active regenerator in its center, a heat exchanger on each side and a driving mechanism used for alternately pushing the fluid back and forth through the regenerator.

The function principle to implement the above stated cooling cycle is depicted in Fig. 1 for a schematic setup of an AER. In the first step, the EC material of the regenerator is activated by applying an electric field. Thus, the temperature of the regenerator increases by ΔT_{ECE} . While the electric field is applied, the fluid is in the second step pushed to the opposite direction, absorbing heat from the regenerator and delivering it to the hot heat exchanger. In the third step, the field is turned off, resulting in a decrease of the regenerator

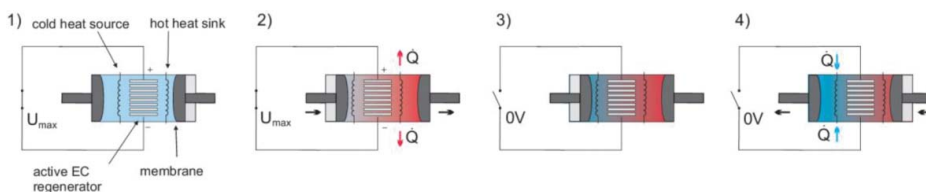


Figure 1. Schematic and function principle of an AER cooling device.

temperature. The fluid is pushed back through the regenerator, expelling heat to the active elements and reaching the cold heat exchanger at a lower temperature. The fluid can then absorb heat and repeat the cycle from the first step. After several cycles, a temperature gradient is established between source and sink (ΔT_{Device}). Due to the regeneration, this temperature difference can be significantly larger than ΔT_{ECE} . Additionally, different material compositions, which are adjusted optimally to the local steady-state operating temperature range, can be used along the length of the regenerator to increase performance.

The specific AER device presented in this paper (Fig. 2) is designed to hold regenerators built from rectangular EC elements. It consists of a channel (1) containing the regenerator made of active material (2) and a heat exchanger on each side (3). The channel is filled with silicon oil, which is pushed through the regenerator plates by pistons separated by membranes (4). Temperature is measured by sensors attached to the heat exchangers. The dimensioning of the regenerator and heat exchanger elements is flexible. This allows the evaluation of different regenerators (material systems, design) and heat exchangers in the same system.

The regenerator evaluated in this paper is made of two stacks of EC elements in series. Each stack holds four equally spaced multi-layer samples. In accordance with the element thickness of 0.8 mm the gap between the samples was determined to be approx. 0.4 mm. It is achieved by small brass spacers which were applied with electrical conductive adhesive so that they can also be used for electrical connection. The schematic design of the regenerator is shown in Fig. 3. Adverse element surfaces always have the same electrical potentials to prevent shorts and dielectric losses from the fluid. Electrical connections are lead through the lid to the outside. The regenerator has a total size of $36 \times 8 \times 5 \text{ mm}^3$ of which a volume of 680 mm^3 (approx. 47%) is the active PMN-PT part that shows the ECE on application of the electrical field.

For initial evaluation, thin film PT1000 resistance thermometers fixed to small brass plates acting as thermal buffer are installed in the place of the heat exchangers. This allows the determination of ΔT_{Device} depending on operational parameters without heat loss via heat exchangers. For extended investigations, temperature sensors can later be replaced by passive heat exchangers or active heat loads (resistance heaters, Peltier elements). The fluid flow through the regenerator is adjusted by the stroke of the membranes. Membranes have been chosen because they allow a precise adjustment of the fluid flow and prohibit heat generation from friction.

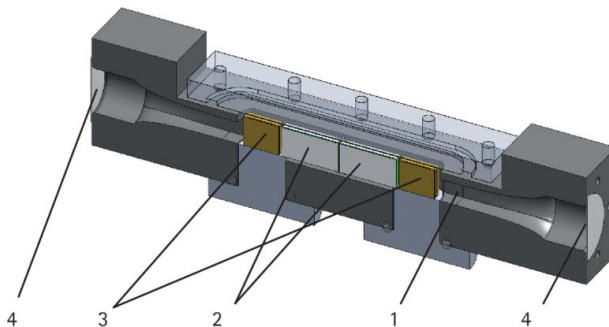


Figure 2. CAD model of developed AER device with fluidic channel (1), regenerator out of active elements (2), heat exchangers (3) and membranes (4).

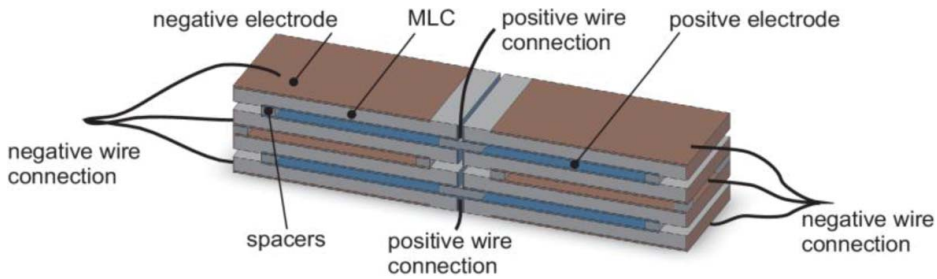


Figure 3. Schematic of regenerator design.

3. Material system

The active elements used in the regenerator are multilayer ceramics (MLC). For their preparation, PMN-8PT green tapes with a thickness of $110\ \mu\text{m}$ were produced by doctor blade process. Therefore, calcined powder was grinded for 6 h in a planetary ball mill at 200 rpm in isopropyl alcohol and then mixed with binder, plasticizer and solvent. Dried green tapes were cut into $90\ \text{mm} \times 90\ \text{mm}$ pieces and Ag/Pd inner-electrodes applied by screen-printing. Multilayer stacks made of seven layers were fabricated by stacking and lamination in an isostatic lamination system. After separation into $22\ \text{mm} \times 10\ \text{mm}$ components by laser cutting and subsequent sintering at $1050\ ^\circ\text{C}$ for 2 h, terminal electrodes of gold were applied by sputtering. In this initial MLC design, the EC elements are MLC samples of $17.8 \times 7.9 \times 0.76\ \text{mm}^3$ (Fig. 4). Each sample consists of 7 layers of $0.92\ \text{Pb}(\text{Mg}_{1/3}\text{Nb}_{2/3})\text{O}_3 - 0.08\ \text{PbTiO}_3$ (PMN-8PT) with a thickness of $95\ \mu\text{m}$ each. The ceramic layers are separated by $3\ \mu\text{m}$ thick electrode layers.

The composition was chosen due to its T_m of around $30\ ^\circ\text{C}$, which is around the destined application temperature of $40\ ^\circ\text{C}$ and the material should thus exhibit a large ECE within this temperature range. Variation of the materials lead titanate content allows for shifting T_m to various temperatures [11], while dopants, e.g. Li^+ , could be added to decrease hysteresis losses [12].

Compared to bulk ceramics, the advantage of the multilayer structures is the increased dielectric strength (7 kV/mm in bulk, 10 kV/mm in MLC) and the reduced layer thickness, resulting in reduced operation voltages. Direct electrocaloric measurement using thermocouples under application/withdrawal of an electric field of 2 kV/mm to the device structures

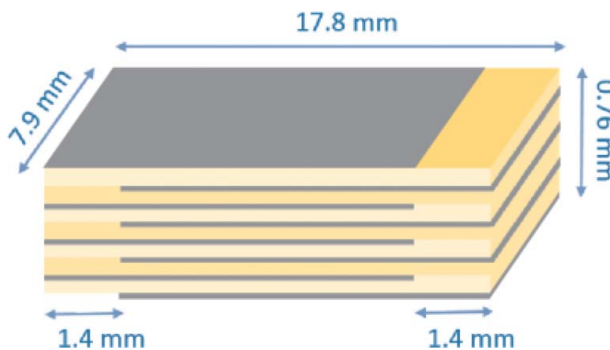


Figure 4. Schematic illustration of the used MLC samples.

showed similar values for both bulk ($\Delta T_{\text{ECE}} = 0.20 \text{ K}$) and multilayer ceramics ($\Delta T_{\text{ECE}} = 0.17 \text{ K}$) (Fig. 5). The bulk ceramic samples used for comparison were prepared as described in [12].

4. Setup and experiments

For the regenerator, multilayer elements, spacers and connecting wires were manually assembled using silver epoxy. After curing, the regenerator was fixed to the lid and the wires were glued in the lid for sealing. To prevent sparkovers, all wires and connection areas were additionally coated with PU. The parts for the housing of the device were printed with a pol-yjet 3D printer. Rubber seals were used to seal the different components and the rubber membranes. The AER was installed between two pistons, which actuate the membranes. The pistons are driven by a stepper motor. A photograph of the final setup is shown in Fig. 6.

For operation, the device is connected to a high voltage source and a stepper motor, both controlled by a LabVIEW controller as depicted in Fig. 7. Measurement values from temperature and voltage sensors from inside the device are continuously acquired with the same program during operation. From the parameter set, the operational parameters lower and upper voltage, cycling frequency and phase shift between fluid displacement and electrical field can be fed to the system. The displacement of the fluid can also be varied but has to be mechanically set.

The experimental evaluation of the operational parameters with different kinds of regenerator designs and active material systems, especially the bulk and multilayer systems, is thus possible with this AER device demonstrator. Unfortunately, due to practical problems only very few measurement data could be obtained so far. These problems can be briefly summarized as follows and should be carefully regarded in any device setup:

–**Insulation.** Insulation of silicon oil alone is not always sufficient. (Surface conductivity, enclosed air bubbles, contamination of fluid). Additional insulation is thus necessary on rims, for multilayers as well as for bulk. A complete insulation of all element surfaces and conductive parts could enable the use of non-dielectric heat transfer fluids as water. The

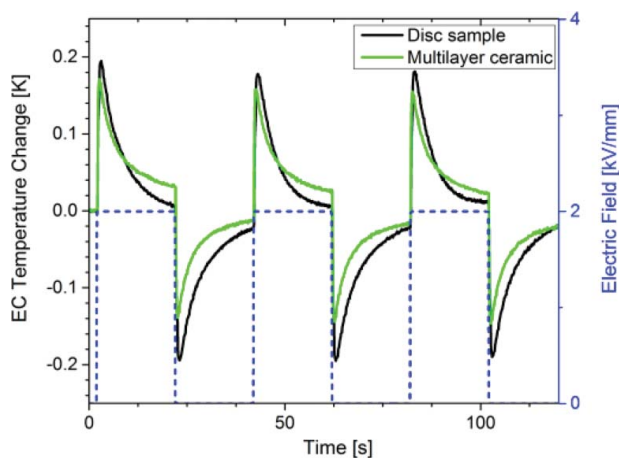


Figure 5. Electrocaloric temperature change of disc shaped bulk ceramic and MLC sample of PMN-8PT at room temperature.

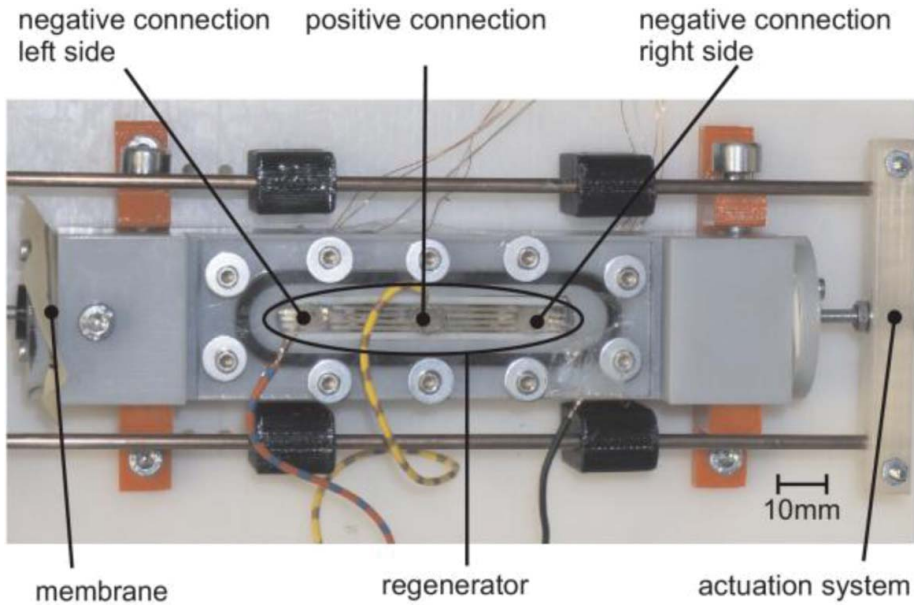


Figure 6. Photograph of build AER device demonstrator.

better thermal properties of such fluids have than to be contrasted against the additional thermal resistance of insulation layers. In our setup, we could improve element stability significantly by additional insulation.

–**Sealing.** Silicon oil is very volatile and any leakage may lead to air in the system. This may not only increase the risk of shorts but also limit heat transfer if the amount of air in the system is significant. As it is not easy to completely avoid air enclosures in setup and seals may weaken during operation, trapping air in designated “safe” positions (e.g. a cavity) and occasional de-airing is, for demonstration systems, acceptable and recommended.

–**Assembling.** Electrical and mechanical connections have to be carefully established to prevent delamination of electrodes, breakdown or unwanted thermal bridges. We also encountered the problem that MLC showed warpage so that the samples in the regenerator and the gap could not be perfectly aligned.

Measurements results could be obtained with the AER device demonstrator and the specified MLC regenerator so far for electric fields up to 1 kV/mm. The ΔT_{ECE} at this field

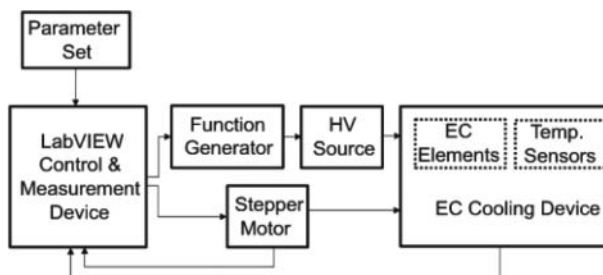


Figure 7. Schematic of control system.

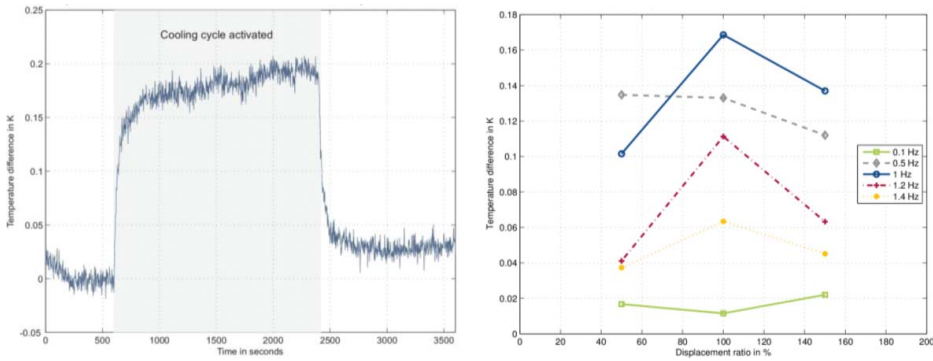


Figure 8. Measurement results. Development of temperature span between hot and cold side of the device at cycling frequency of 1 Hz, $E = 1$ kV/mm and displacement ratio of 1, max. $\Delta T_{\text{Device}} = 0.17$ K (left), ΔT_{Device} in dependence from fluid displacement ratio and frequency at $E = 1$ kV/mm (right).

strength is approx. 0.009 K. The differential curve of the temperatures on hot and cold sides of the regenerator (Fig. 8) clearly shows the development of a temperature span during operation of the device.

The amount of fluid displacement has been varied between 50% and 150% of the fluidic volume in contact with the active regenerator, i.e. at 50% displacement ratio the fluid is pushed in one cycle from one end of the regenerator to its middle and back again. The cycling frequency has been elaborated in the range from 0.1 Hz to 1.4 Hz. The maximum temperature span achieved within the elaborated parameter range was nearly $\Delta T_{\text{Device}} = 0.17$ K at $E = 1$ kV/mm, $f = 1$ Hz and displacement ratio of 1 (Fig. 8). Even though this absolute value is fairly low, taking into account the low ΔT_{ECE} of 0.009 K, this however represents a regeneration factor of almost 2. The ΔT_{Device} can be further increased by increasing E and increasing the regeneration factor. The increase of E to 2 kV/mm already leads to a doubling of ΔT_{ECE} and thus ΔT_{Device} . A prospective further increase up to the breakdown field will further increase the temperature span. The regeneration factor can be increased by a larger active heat capacity (i.e. more elements to reduce influences on thermal losses) and larger regenerator length or other heat transfer fluids [8]. Taking into account the differences of the active regenerator volumes and the different electrical fields applied, these first results generally conform to results presented by Plaznik et al. [8].

5. Conclusion

In this paper, an AER device demonstrator has been presented, which allows the direct comparison of different EC materials and regenerator designs in the same system. Relaxor PMN-8PT MLC systems are currently being assessed with this device. First results show a temperature span over the device of twice the size of the ECE of the active material. This proves the functionality of the device and the material but does not reveal any of the expected advantages of MLC over bulk material. However, the advantages of the MLC, especially the higher breakdown strength, could not be exploited so far, since premature failure of the regenerator prevented further evaluation. Extensive evaluation of MLC will be done with a new regenerator out of the presented samples in the developed device to exploit these

advantages and systematically analyze the influence of fluid displacement ratio, cycling frequency, electric field strength and phase shift between field application and displacement. For future research, the electrode layout of MLC samples will be further improved by adding a small insulating border to allow for application of higher electric fields and thus obtain higher EC temperature changes. Expectedly, this will also reduce current insulation problems in the regenerator.

Two further aspects will have to be regarded in future research. For any application, larger regenerator assemblies will be necessary and the capacitance will significantly increase. Electrical control and setup will become interesting (controlling charging times and currents). Additionally, the losses in elements and connections have to be minimized, which otherwise inevitably lead to a continuous heating of the systems.

Funding

We would like to thank the German Research Foundation (DFG) for funding this research project in the framework of SPP 1599 Caloric Effects in Ferrioc Materials: New Concepts for Cooling (RA 1736/13-1, GE 2078/3-1).

References

1. W. II. Thomson, On the thermoelastic, thermomagnetic, and pyroelectric properties of matter. *Philosophical Magazine Series 5* **5**(28), 4–27 (1878).
2. P. Kobeko, J. Kurtschatov, Dielektrische Eigenschaften der Seignettesalzkrystalle. *Z. Physik* **66**(3–4), 192–205 (1930).
3. A. S. Mischenko, Q. Zhang, J. F. Scott, R. W. Whatmore, N. D. Mathur, Giant Electrocaloric Effect in Thin-Film $\text{PbZr}_{0.95}\text{Ti}_{0.05}\text{O}_3$. *Science* **311**(5765), 1270–1 (2006).
4. R. I. Epstein, K. J. Malloy, Electrocaloric devices based on thin-film heat switches. *J Appl Phys* **106**(6), 064509 (2009).
5. M. Ožbolt, A. Kitanovski, J. Tušek, A. Poredoš, Electrocaloric vs. magnetocaloric energy conversion. *Int J of Refrigeration* **37**, 16–27 (2014).
6. Y. V. Sinyavsky, V. M. Brodyansky, Experimental testing of electrocaloric cooling with transparent ferroelectric ceramic as a working body. *Ferroelectrics* **131**(1), 321–5 (1992).
7. D. Guo, J. Gao, Y. Yu, S. Santhanam, A. Slippey, Fedder G. K., A. J. McGaughey, S. Yao, Design and modeling of a fluid-based micro-scale electrocaloric refrigeration system. *Int J Heat and Mass Transfer* **72**, 559–64 (2014).
8. U. Plaznik, A. Kitanovski, B. Rožič, B. Malič, H. Uršič, S. Drnovšek, J. Cilensek, M. Vrabelj, A. Poredoš, Z. Kutnjak, Bulk relaxor ferroelectric ceramics as a working body for an electrocaloric cooling device. *Appl Phys Lett* **106**(4), 043903 (2015).
9. P. Blumenthal, A. Tornow, K. Dröder, A. Raatz, Electrocaloric-Cooling in E-Mobility. Proc 4th Int C Ferromagnetic Shape Memory Alloys (2013).
10. C. Neusel, G. A. Schneider, Size-dependence of the dielectric breakdown strength from nano- to millimeter scale. *J Mech Phys Solids* **63**, 201–213 (2014).
11. S. W. Choi, T. R. Shrout, S. J. Jang, A. S. Bhalla, Dielectric and pyroelectric properties in the $\text{Pb}(\text{Mg}_{1/3}\text{Nb}_{2/3})\text{O}_3\text{-PbTiO}_3$ system. *Ferroelectrics* **100**, 29–38 (1989).
12. C. Molin, M. Sanlialp, V. V. Shvartsman, D. C. Lupascu, P. Neumeister, A. Schönecker, S. Gebhardt, Effect of dopants on the electrocaloric effect of $0.92 \text{Pb}(\text{Mg}_{1/3}\text{Nb}_{2/3})\text{O}_3\text{-}0.08 \text{PbTiO}_3$ ceramics. *J Eur Ceram Soc* **35**, 2065–2071 (2015).